RESEARCH REPORT

External Research Program

Moisture and Frost in Fiberglass Insulation

Canada

CMHC SCHL

HOME TO CANADIANS

CMHC—HOME TO CANADIANS

Canada Mortgage and Housing Corporation (CMHC) has been Canada's national housing agency for more than 60 years.

Together with other housing stakeholders, we help ensure that Canada maintains one of the best housing systems in the world. We are committed to helping Canadians access a wide choice of quality, affordable homes, while making vibrant, healthy communities and cities a reality across the country.

For more information, visit our website at **www.cmhc.ca**

You can also reach us by phone at 1-800-668-2642 or by fax at 1-800-245-9274.

Outside Canada call 613-748-2003 or fax to 613-748-2016.

Canada Mortgage and Housing Corporation supports the Government of Canada policy on access to information for people with disabilities. If you wish to obtain this publication in alternative formats, call 1-800-668-2642.

MOISTURE AND FROST IN FIBERGLASS INSULATION

Moisture and Frost in Fiberglass Insulation

By Robert W. Besant and Yong-Xin Tao

Department of Mechanical Engineering
University of Saskatchewan

April, 1992

CMHC Project Manager: Tom Hamlin, Research Division

This project was carried out with the assistance of a grant from Canada Mortgage and Housing Corporation under the terms of the External Research Program (CMHC CR File 6585/B82). The views expressed are those of the authors and do not represent the official views of the Corporation.

Executive Summary

In millions of houses and residential dwellings in Canada, fiberglass insulation is the prime material used to protect the inhabitants from large variations in ambient temperatures. Fiberglass insulation, when exposed to transient conditions of temperature and humidity, exhibits physical phenomena that are not well understood, although, in practice, the consequences of the failure of vapor retarders in air-tight structures due to installation problems (among other factors) are known in the design and consulting communities [1]. Only in the last few years have studies been conducted presenting experimental data and theoretical models for predicting moisture accumulation in fiberglass insulation [1-8]. For applied temperature ranges above the freezing point, it has been shown that the additional, steady-state heat loss, due to condensation of water in an insulation slab under a thermal gradient, is negligible if the mass transport process in the slab is dominated by vapor molecular diffusion is small [5]. This conclusion is supported by an experimental study by Kumaran [4] in which a glass-fiber insulation slab, after being open to a moist air at 97% relative humidity for a long time, showed no significant increase in heat flux as compared to a dry slab. It has also been reported by Wijeysundera et al. [5], for an insulation slab with its impermeable cold side (an ideal vapor "barrier" applied) and the warm side open to a forced convective moist air at a relative humidity of less than 80%, the heat loss is almost the same as if the slab is dry. However, when the cold side of the insulation slab is subject to a temperature below the triple point of water, condensed water may exist as frost which both alters the temperature distribution and increases the effective thermal conductivity of the slab. A numerical study [9] shows that condensation and frosting in a typical glass-fiber slab will result in a 10 to 30% increase in heat flux at the quasi-steady-state when the ambient air relative humidity is above 60 %.

In all the predictions mentioned above, the hygroscopicity of the glass-fiber insulation was not considered in the models. Condensation, or frosting, is assumed to occur when the local vapor density reaches its saturation value, i.e. no water vapor adsorption is considered. Mitalas and Kumaran [10] made an estimate of the hygroscopic effects for a glass-fiber slab in a closed system; their test facility contained a fixed quantity of water and vapor in a sealed cell and was not exposed to ambient moist air. They concluded that the hygroscopic effects on the thermal performance was negligible when this wrapped slab was subject to a temperature difference in their heat flow measurement apparatus. However, a previous experimental work [11] shows that, when an initially oven-dried glass-fiber slab has one side open to moist air and is subjected to a large temperature difference across the slab, the measured internal slab temperatures and heat flux from the cold surface are higher than those predicted using a model that excludes the hygroscopicity effects. Furthermore, it was found that only for a slab, that was initially wetted, were the measured temperature and heat flux close to the prediction. These observations indicate that the hygroscopicity in fiber-glass insulation may have a strong effect on its transient thermal performance.

Résumé

L'humidité et le givre dans l'isolant en fibre de verre

L'isolant en fibre de verre est le matériau le plus utilisé dans des millions d'habitations canadiennes pour protéger les occupants contre les larges écarts de température ambiante. Lorsqu'elle est exposée à des conditions de température et d'humidité transitoires, la fibre de verre subit des transformations physiques qui sont mal connues. Dans la pratique, toutefois, les concepteurs et les consultants oeuvrant dans ce domaine connaissent les conséquences de la défaillance du pare-vapeur dans un bâtiment étanche à l'air découlant d'une mauvaise installation (entre autres facteurs)[1]. Or, ce n'est que depuis quelques années que des études ont commencé à fournir des données expérimentales et des modèles théoriques permettant de prévoir l'accumulation d'humidité dans l'isolant en fibre de verre[1,8]. Lorsque les échelles de température appliquées dépassent le point de congélation, il s'avère que la perte de chaleur additionnelle en régime permanent engendrée par la condensation de l'eau à l'intérieur d'une plaque d'isolant sous gradient thermique est négligeable si le procédé de transport de masse dans la plaque est dominé par la diffusion moléculaire de la vapeur[5]. Cette conclusion s'appuie sur une étude expérimentale de Kumaran[4] selon laquelle une plaque d'isolant en fibre de verre ayant été longtemps exposée à de l'air dont l'humidité relative était de 97 p. 100 n'a présenté aucune élévation significative du flux thermique par rapport à une plaque sèche. Wijeysundera et coll.[5] signalent aussi que, pour une plaque d'isolant dont le côté imperméable froid (un pare-vapeur idéal étant mis en oeuvre) et le côté chaud sont exposés à un air humide convectif pulsé à une humidité relative de moins de 80 p. 100, la perte de chaleur est presque la même que si la plaque était sèche. Cependant, lorsque le côté froid de la plaque d'isolant est soumis à une température inférieure au point triple de l'eau, l'eau peut s'y condenser sous forme de givre, modifiant ainsi la distribution de la température et accroissant la conductivité thermique réelle de la plaque. Une étude numérique[9] montre que la condensation et le givre se formant dans une plaque typique d'isolant en fibre de verre occasionnent une augmentation de 10 à 30 p. 100 du flux de chaleur en régime quasi constant lorsque l'humidité relative de l'air ambiant est supérieure à 60 p. 100.

Aucun des modèles prévisionnels mentionnés ci-dessus ne tient compte de l'hygroscopicité de l'isolant en fibre de verre. On présume que la condensation, ou le givre, survient lorsque la densité locale de la vapeur atteint son point de saturation, c'est-à-dire qu'aucune adsorption de vapeur d'eau n'est considérée. Mitalas et Kumaran[10] ont évalué les effets hygroscopiques d'une plaque de fibre de verre dans un système clos. Leur installation d'essai était constituée d'une quantité fixe d'eau et de vapeur à l'intérieur d'une cellule close à l'abri de l'air humide ambiant. Ces chercheurs concluent que les effets hygroscopiques sur le comportement thermique sont négligeables lorsque cette plaque enveloppée est soumise à une différence de température dans leur appareil de mesure du mouvement de la chaleur. Par ailleurs, une expérience antérieure a montré[11] que lorsqu'une plaque d'isolant de fibre de verre préalablement séchée au four était exposée à de l'air humide sur un côté et soumise entièrement à une grande différence de température, les températures mesurées à l'intérieur de la plaque et du flux thermique sur la surface froide sont supérieures à celles qui sont

prévues à l'aide d'un modèle excluant les effets hygroscopiques. En outre, on a constaté que les températures et le flux thermique mesurés n'ont été comparables aux prévisions que dans le cas d'une plaque qui avait d'abord été mouillée. Ces observations révèlent que l'hygroscopicité de l'isolant en fibre de verre peut avoir un effet important sur son comportement thermique transitoire.

National Office
700 Montreal Road
Ottawa ON K1A 0P7
Telephone: (613) 748-2000

Bureau national
700 chemin de Montréal
Ottawa ON K1A 0P7
Téléphone : (613) 748-2000

Puisqu'on prévoit une demande restreinte pour ce document de recherche, seul le résumé a été traduit.

La SCHL fera traduire le document si la demande le justifie.

Pour nous aider à déterminer si la demande justifie que ce rapport soit traduit en français, veuillez remplir la partie ci-dessous et la retourner à l'adresse suivante :

Centre canadien de documentation sur l'habitation
Société canadienne d'hypothèques et de logement
700, chemin Montréal, bureau C1-200
Ottawa (Ontario)
K1A 0P7

Titre du rapport: _____

_____

Je préférerais que ce rapport soit disponible en français.

NOM _____

ADRESSE _____
rue App.

_____
ville province Code postal

No de téléphone ( ) _____

CONTENTS

List of Figures

List of Tables

1 INTRODUCTION

In millions of houses and residential dwellings in Canada, fiberglass insulation is the prime material used to protect the inhabitants from large variations in ambient temperatures. Fiberglass insulation, when exposed to transient conditions of temperature and humidity, exhibits physical phenomena that are not well understood, although, in practice, the consequences of the failure of vapor retarders in air-tight structures due to installation problems (among other factors) are known in the design and consulting communities [1]. Only in the last few years have studies been conducted presenting experimental data and theoretical models for predicting moisture accumulation in fiberglass insulation [1-8]. For applied temperature ranges above the freezing point, it has been shown that the additional, steady-state heat loss, due to condensation of water in an insulation slab under a thermal gradient, is negligible if the mass transport process in the slab is dominated by vapor molecular diffusion is small [5]. This conclusion is supported by an experimental study by Kumaran [4] in which a glass-fiber insulation slab, after being open to a moist air at 97% relative humidity for a long time, showed no significant increase in heat flux as compared to a dry slab. It has also been reported by Wijeysundera et al. [5], for an insulation slab with its impermeable cold side (an ideal vapor "barrier" applied) and the warm side open to a forced convective moist air at a relative humidity of less than 80%, the heat loss is almost the same as if the slab is dry. However, when the cold side of the insulation slab is subject to a temperature below the triple point of water, condensed water may exist as frost which both alters the temperature distribution and increases the effective thermal conductivity of the slab. A numerical study [9] shows that condensation and frosting in a typical glass-fiber slab will result in a 10 to 30% increase in heat flux at the quasi-steady-state when the ambient air relative humidity is above 60 %.

In all the predictions mentioned above, the hygroscopicity of the glass-fiber insulation was not considered in the models. Condensation, or frosting, is assumed to occur when the local vapor density reaches its saturation value, i.e. no water vapor adsorption is considered. Mitalas and Kumaran [10] made an estimate of the hygroscopic effects for a glass-fiber slab in a closed system; their test facility contained a fixed quantity of water and vapor in a sealed cell and was not exposed to ambient moist air. They concluded that the hygroscopic effects on the thermal performance was negligible when this wrapped slab was subject to a temperature difference in their heat flow measurement apparatus. However, a previous experimental work [11] shows that, when an initially oven-dried glass-fiber slab has one side open to moist air and is subjected to a large temperature difference across the slab, the measured internal slab temperatures and heat flux from the cold surface are higher than those predicted using a model that excludes the hygroscopicity effects. Furthermore, it was found that only for a slab, that was initially wetted, were the measured temperature and heat flux close to the prediction. These observations indicate that the hygroscopicity in fiber-glass insulation may have a strong effect on its transient thermal performance.

It is known that physical adsorption and capillary condensation are the main mechanisms of phase change during hygroscopic mass transfer in glass-fiber materials [6,12]. The hygroscopicity (here we only deal with water vapor) for a material is traditionally characterized by empirical, equilibrium adsorption or desorption isotherms. These isotherms represent the amount of vapor adsorbed at thermodynamic equilibrium conditions as a function of the relative humidity of the moist air. It is known that, besides temperature and relative humidity, the capacity for adsorption strongly depends on the percentage and type of bonding materials used in making insulation boards and is also a function of the glass-fiber diameter (or specific surface area) and insulation bulk density. Applying this knowledge to a relatively thick insulation slab, subject to a thermal

gradient and assuming local thermodynamic equilibrium, we can conclude that phase change occurs by adsorption or desorption even when the local relative humidity is less than 100%. For the local relative humidity between 90 to 100 %, capillary condensation may occur depending on the local pore structure. Furthermore, phase change mass transfer is coupled with heat transfer during an adsorption process; i.e., the energy that equals the mass of adsorption multiplied by the enthalpy of adsorption is released, acting as a heat source. Since the enthalpy of adsorption is usually larger than the enthalpy of condensation, it is expected that the transient temperature field in the slab will be different from that in a glass-fiber slab using only the heat of condensation. During a transient thermal response test, these hygroscopic effects are expected to be stronger for an initially dry sample that is subject to a large temperature difference across it [13].

In this report, the progressive research results, under the External Research Contract (1990-1991) sponsored by CMHC, are summarized. The original three main objectives of this research contract are:

1. Using our test facility to measure the heat of adsorption in typical fiberglass products under a range of temperature and humidity conditions within accurately monitored laboratory conditions.

2. Using the measured data from Objective (1) to develop a time-dependent, one-dimensional theoretical/numerical model that combine adsorption/desorption, condensation/evaporation, and ablimation/sublimation with water vapor diffusion in fiberglass insulation.

3. Validate the accuracy of this model, (2), using our existing cold temperature laboratory test facility for a few independent experiments involving the same physical phenomena described in Objective (2).

In the following, we first present the experimental study of measuring the heat of adsorption. A transient, one-dimensional model for simultaneous heat and mass transfer with phase changes for a fibrous medium to predict the spatial and temporal variation of the temperature, water volume fraction, vapor density, and rate of phase change, using the measured heat of adsorption, is then described, and the typical predictions are discussed. Finally, the prediction will be compared with the results obtained from the experiments.

2 MEASUREMENT OF THE HEAT OF ADSORPTION

It is known that the physical adsorption of a gas (here we deal with water vapor) on a solid surface is always accompanied by the evolution of thermal energy. This heat of adsorption has to be defined by giving the initial and final thermodynamic states of the adsorptive system and the conditions under which any heat flux takes place; examples are adiabatic heat of adsorption, isosteric heat of adsorption, etc. [14]. The most commonly used phase-change heat in engineering-related problems is the isosteric heat of adsorption (or alternatively, the isosteric enthalpy of adsorption), which can be expressed in the same form as the enthalpy of condensation (or sublimation) in the Clapeyron equation [13]. In thermodynamic terms, the isosteric heat of adsorption is the differential enthalpy of adsorption (as compared to the definition of the integral enthalpy of adsorption). This allows us to use it in solving the differential energy equation. In general, the isosteric heat of adsorption has the following functional form:

$$h_{\mathrm{ad}} = f(W, T, \text{adsorptive gas, adsorbent solid}), \tag{1}$$

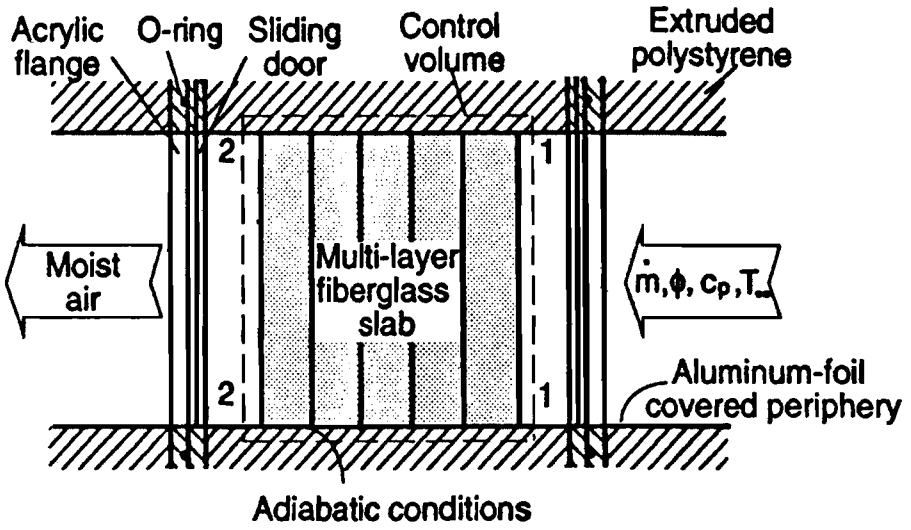

Figure 1: The test section for measuring the heat of adsorption. Indicated also is the control volume for the derivation of the measurement principle.

where W is the equilibrium mass of the adsorbate and T is the absolute temperature. Since the adsorption isotherms for a given adsorptive-adsorbent system can be expressed as a function of relative humidity, ϕ, and temperature, T, i.e.,

$$W = f(\phi, T), \tag{2}$$

Equation (1) is also written as

$$h_{ad} = f(\phi, T). \tag{3}$$

Many methods are reported in the literature for measurement of different heats of adsorption [14]. Most of them are designed for a pure adsorptive gas (not like an air-water vapor mixture) using very complicated test apparatus and requiring a very long test time. They are usually very accurate (examples are the calorimetric method and chromatography method). In this study, we develop a relatively simple method that is more suitable for highly porous insulation materials and still yields a reasonable accuracy.

Consider a control volume, as shown in Figure 1, consisting of an insulation matrix, which undergoes an adsorption process. At the initial state, the temperature of the system is T_1 and the relative humidity is nearly zero. At the starting time $t = 0^+$, a steady moist airflow at temperature T_1, relative humidity $\phi > 0$, and mass flow rate $\dot{m}_a$ enters and leaves the control volume. A part of the water vapor in the airstream is then adsorbed on the glass-fiber surfaces. The evolved heat is carried away downstream by the airflow, causing the temperature at the outlet of the control volume, T_2, first to rise and later to fall. At the final state, time= t, the control volume is again in thermodynamic equilibrium with the surroundings, at T_1 and ϕ. The application of the first law of thermodynamics yields the following:

$$\int_0^t [\dot{m}_a c_{pa}(T_2 - T_1) - \left.\frac{\partial H}{\partial t}\right|_{cv} - \dot{m}_{ad} h_{ad}]dt = 0, \tag{4}$$

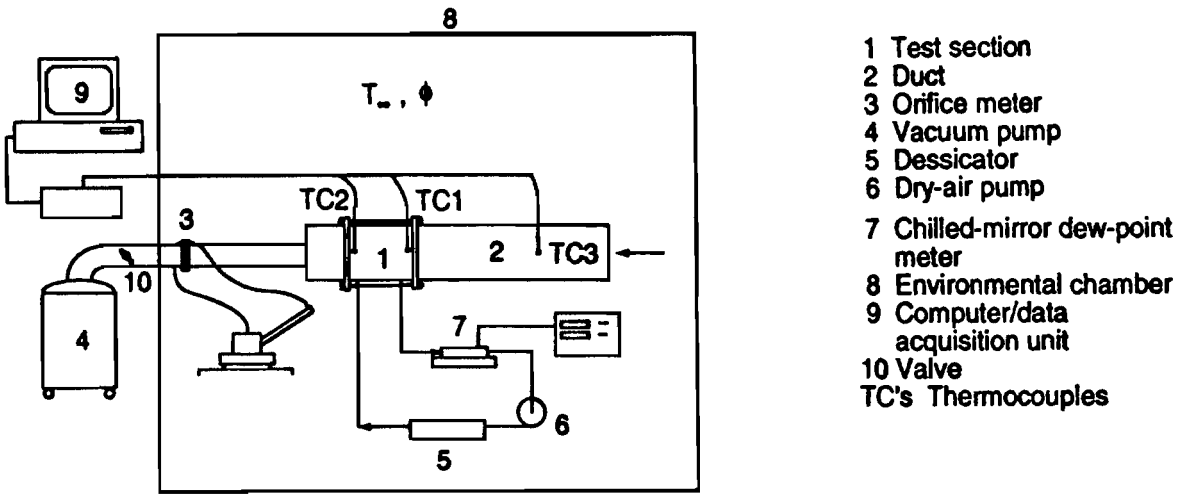

Figure 2: A schematic of the experimental apparatus for measuring the heat of adsorption.

where c_{pa} is the specific heat of air, $\dot{m}_a$ is the mass flow rate, H_{cv} is the total enthalpy of the control volume excluding the adsorbate, $\dot{m}_{ad}$ is the rate of adsorption, and h_{ad} is the heat of adsorption. The mass conservation applied to the control volume, including the adsorbate, gives

$$m_{cv,t} - m_{cv,0} = \Delta m. \tag{5}$$

Since the temperature of the system at the final state is the same as at the initial state, we have

$$\int_0^t \left.\frac{\partial H}{\partial t}\right|_{cv} dt = H_{cv,t} - H_{cv,0} = 0.$$

If $\dot{m}_a$ is independent of time and c_{pa} can be treated as a constant, then Equation (4) becomes (after some algebraic manipulation)

$$\bar{h}_{ad} = \frac{c_{pa}\dot{m}_a S}{\Delta m}, \tag{6}$$

where $\bar{h}_{ad}$ is the average heat of adsorption with respect to Δm, and $S = \int_0^t (T_2 - T_1)dt$ is the adsorption temperature signature. Equation (6) is the theoretical basis for the design of the heat of adsorption apparatus; the apparatus should be able to provide a steady, moist airflow, keep the ambient temperature constant, ensure the final temperature of the system is equal to the initial temperature, and finally, be able to get a significant, accurate reading of S.

It is noted that since the definition of the average heat of adsorption in Equation (6) includes the total mass of water vapor adsorbed from some initial state at temperature T_1 and relative humidity ϕ_0 to a final state T_1 and ϕ, the heat released at any intermediate state will not, in general, equal the average heat of adsorption and the rate of adsorption will not be a constant. To get thermodynamic state heat of adsorption, we can write the average heat of adsorption as a function of adsorbed water vapor, W, by choosing a proper form of correlation,

$$\bar{h}_{ad} = f(W), \tag{7}$$

so that we can write

$$h_{ad} = \frac{\partial W \bar{h}_{ad}}{\partial W} = \bar{h}_{ad} + W \frac{\partial \bar{h}_{ad}}{\partial W}, \tag{8}$$

where, by definition

$$\bar{h}_{ad} = \frac{1}{W} \int_0^W h_{ad} dW.$$

From the measured average heat of adsorption (Equation (7)), the thermodynamic state heat of adsorption, $h_{ad}(\phi, T)$, can then be determined using Equation (8). For comparison with the heat of vaporization, we will discuss the results in terms of the ratio of the heat of adsorption to the heat of vaporization, i.e.,

$$h' = \frac{h_{ad}}{h_{fg}} \text{ or } \bar{h}' = \frac{\bar{h}_{ad}}{h_{fg}}.$$

2.1 Apparatus

The test section and apparatus are shown in Figures 1 and 2. The test section has a cross-sectional area of 17 by 17 cm for mounting the insulation sample. The multilayer sample has a thickness between 8 cm and 10 cm, depending on the sample bulk density. The test section and the duct are made of extruded polystyrene boards with a thickness of 1 inch (2.54 cm) to ensure an adiabatic boundary condition. There are two sliding-door assemblies placed on the upstream and downstream sides of the test section. By closing the sealed doors (using a vacuum grease), the sample can be dried through a desiccator-air loop, shown in Figure 2.

The inner surface of the duct, upstream and downstream, is covered by aluminum foil to minimize the possible thermal radiation to the thermocouples. Thermocouples are mounted at the upstream location (TC3) of the duct and at about 3 to 4 mm away from the sample surfaces that face the upstream (TC1) and downstream (TC2) of the duct, respectively. Further downstream of this wind tunnel, an orifice meter, designed according to ISO standards, is connected to measure the airflow rate. The orifice meter has a discharge coefficient of 0.604 for the mass flow rate of 2.4×10^{-3} kg/s, and its orifice diameter is 12.5 mm. A standard calibration procedure is performed to obtain the relation between the mass flow rate and meter output. A vacuum pump, as used in an industrial vacuum cleaner, is connected to the downstream end of the wind tunnel, providing a desired airflow through a valve in a suction mode. Compared with the blowing mode, this arrangement eliminates the undesired energy dissipation from the fan and motor being added to the flow. The whole apparatus, except the vacuum, is placed in an environmental chamber that gives controllable ambient conditions for required temperature and relative humidity. The ambient temperature can be controlled within ± 0.1 °C for the temperature range of -20 °C to 40 °C, and the relative humidity within ±5 % from 10 % to 95 %. An electronic scale, with a resolution of 0.01 g and a maximum measurable weight of 3,000 g, is used to weigh the mass of the test section before and after each test.

The directly measured quantities are the temperatures, mass of the test section, and the mass flow rate of air. The design for the test section, the orifice meter and selection of the scale are based on the maximization of the signal output, S (Equation 6), and reduction of the individual measurement errors. With the present design, the maximum temperature increase, $\Delta T = T_2 - T_1$, can be achieved at about 1 °C to 2.8 °C, depending on the relative humidity.

2.2 Test Procedure

The environmental chamber is set at the desired temperature and relative humidity. The closed test section with the mounted glass-fiber insulation is then dried by operating the dry-air loop. It normally takes at least eight hours to have the relative humidity within the test section reduced to 1.5 % to 2.5 %. Within this time frame, the temperatures in the whole system have become constant within $\pm 0.1^{o}$C of the controlled chamber temperature. The mass of the test section at the dry state is measured using the scale that is also located inside the environmental chamber. The test section is then placed in the middle part of the duct and bolted to the flanges on the duct (sealed by dry O-rings). The sliding doors are opened and the vacuum pump for airflow is turned on at the same time. Meanwhile, the computer starts to record the time variation of the thermocouple readings at various locations. The time interval between readings is 1.5 seconds. The test is monitored through the thermocouple output on the computer screen and all the data are recorded on disk. When thermocouple 1 and thermocouple 2 (Figure 2) are shown to reach the same value (within $< 0.05^{o}$C), the sliding doors are once again closed, and the airflow is shut off. The test section is carefully disconnected from the duct and weighed again. During this process, the output of the orifice meter, in terms of pressure drop, is constant and read off for later data reduction. A single test takes about 6 to 10 minutes.

The above procedure is repeated for tests at other sets of temperature and relative humidity. To speed up data collection, several test sections were made and could be dried at the same time, thus permitting the testing of several samples with different densities for the same setting of temperature and relative humidity or checking the repeatability of measurement.

2.3 Typical Results

The apparatus is capable of measuring the heat of adsorption for different density insulation samples in a fairly large range of temperature and humidity. In the following, we report the results for two samples with different densities. The basic physical data are listed in Table 1. The error analysis for the apparatus and measurements were discussed in ref. [16].

In Figures 3 and 4, the typical adsorption signals, $\Delta T = T_2 - T_1$, are shown as a function of the test time. The other measured quantities for these two examples are tabulated in Table 3. When a test starts, temperature T_2 rises significantly (recall T_1 is kept constant). In the typical test result shown in Figure 3, ΔT decreases after $t = 60$ s and asymptotically reaches zero at about 560 s. The time for the peak temperature difference becomes shorter when the test is run at a low relative humidity or low temperature. Thus, in general, the maximum ΔT is larger for a high relative humidity than that for a low relative humidity. The area under the ΔT curve (Figure 3 or 4) is equal to S, defined in Equation (6), which is integrated numerically from the discrete temperature readings (e.g., for a 10 minute test, there are about 375 data points).

The measured average heat of adsorption for two samples (different bulk densities) is shown in Figure 5, plotted as $\bar{h}'$ versus W, where W is the percentage of vapor adsorbed (mass basis), defined as

$$W = \frac{\Delta m}{m} \times 100$$

(m is the total mass of the dry sample, $\phi_0 < 2.5\%$) and $\bar{h}'$ is the ratio of the average heat of adsorption to the heat of vaporization at the same temperature (Equation (7)). For the temperature range from 5 °C to 30 °C, all data are seen to be within $\pm 20\%$ of a curve, i.e., no significant temperature

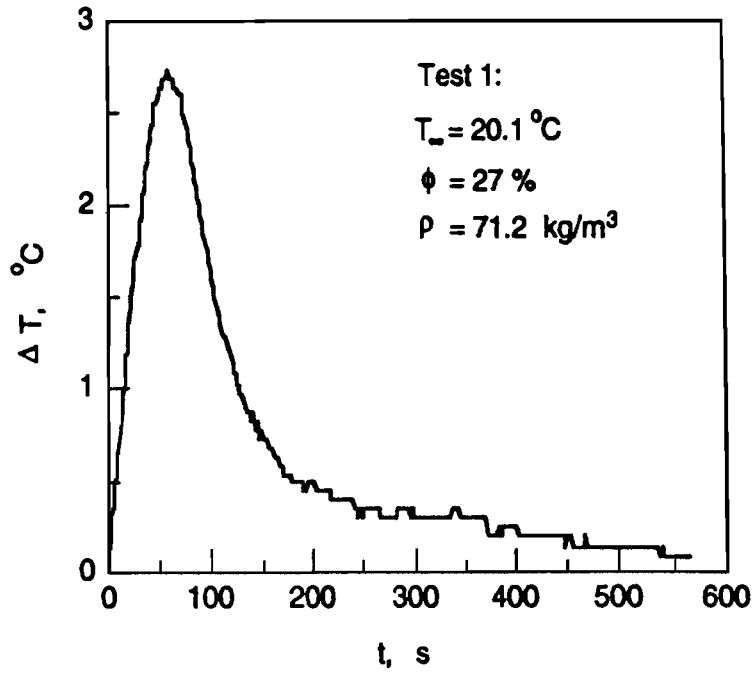

Figure 3: The typical time variation of the temperature output for $\rho = 71.2$ kg/m^3.

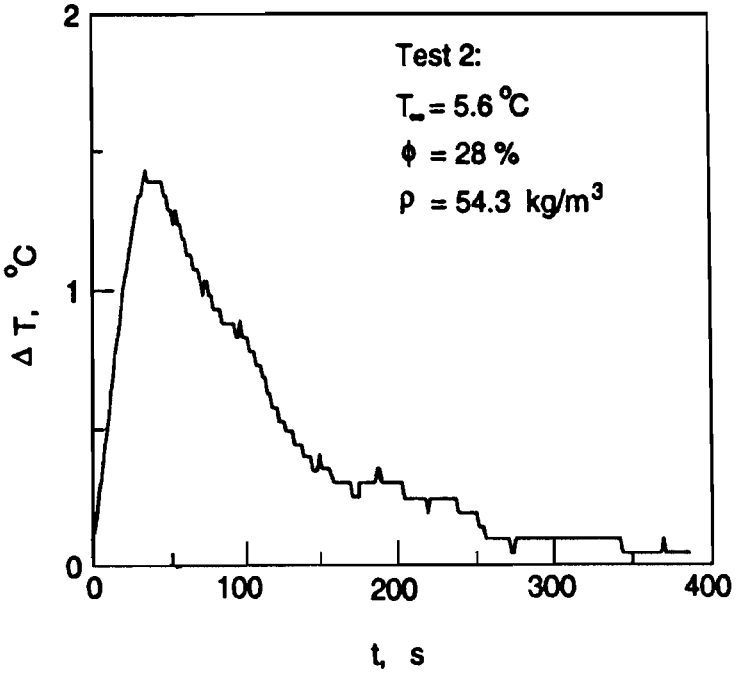

Figure 4: The typical time variation of the temperature output for $\rho = 54.3$ kg/m^3.

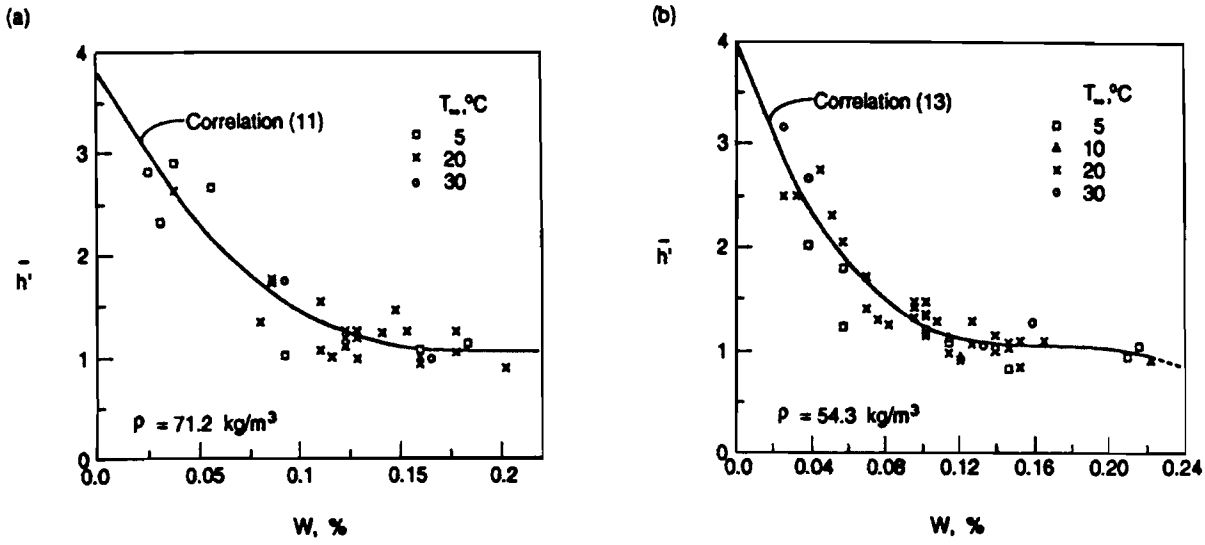

Figure 5: The ratio of the average heat of adsorption to the heat of vaporization as a function of Δm: (a) $\rho = 71.2$ kg/m^3 and (b) $\rho = 54.3$ kg/m^3.

dependency is observed for the heat of adsorption over this temperature range . As expected, $\bar{h}'$ is always greater than unity (within the measurement error) and becomes larger for low W. For example, $\bar{h}'$ is about 3 for $W = 0.06$ %. This confirms the results by Tao et al. (1991b) that for an initially dry fiberglass insulation slab subject to a moist air convection boundary condition on one side and a subfreezing temperature on the others, a hygroscopic, transient thermal response with a temperature rise occurs when W is of the order of 0.05 %. As the adsorbed mass increases, the heat of adsorption approaches the value of the heat of vaporization; i.e., $\bar{h}'$ becomes unity. Physically, low W values correspond to the case where only a single molecular layer of adsorbate phase is on the solid (adsorbent) or the adsorbate partially covers the solid; therefore, the energy exchange is essentially between the adsorptive (gaseous) phase and adsorbent (solid) molecules that form a tighter bond between each other than between vapor and liquid molecules. Further deposition of the adsorbate increases the interaction between the adsorbate and adsorptive such that eventually, the energy exchange would be basically between the vapor and liquid (a stage called capillary condensation).

Also seen from Figure 5, the difference between the result for $\rho = 71.2$ kg/m^3 and that for $\rho = 54.3$ kg/m^3 is very small. A least-squares curve fitting gives the following correlations for the average heat of adsorption (shown in Figure 5) and differential heat of adsorption (Equation (8)): For $\rho = 71.2$ kg/m^3,

$$\bar{h}' = 3.804 - 40.128W + 191.024W^2 - 295.776W^3, \quad 0 \le W \le 0.28\%, \tag{9}$$

$$h' = 3.804 - 80.256W + 573.072W^2 - 1183.104W^3, \quad 0 \le W \le 0.1\%. \tag{10}$$

For $\rho = 54.3$ kg/m^3,

$$\bar{h}' = 4.003 - 53.298W + 319.044W^2 - 635.594W^3, \quad 0 \le W \le 0.22\%, \tag{11}$$

$$h' = 4.003 - 106.596W + 957.132W^2 - 2542.376W^3, \quad 0 \le W \le 0.07\%. \tag{12}$$

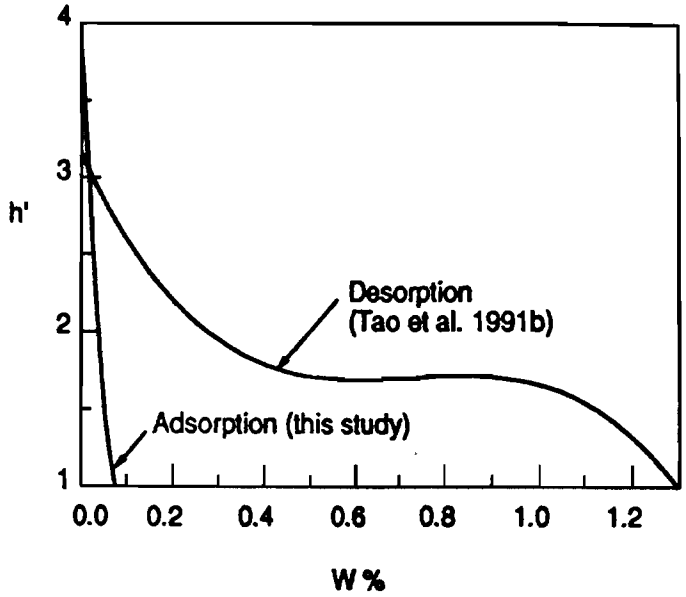

Figure 6: Comparison of the heat of adsorption with the heat of desorption.

We also have

$$\bar{h}' = 1, \ W > 0.28\%, \text{ and } h' = 1, \ W > 0.1\%. \tag{13}$$

The above equations should be limited to the temperature range from 5 °C to 30 °C. The coefficients of the above equations for different densities are very close, which means that the heat of adsorption is basically independent of the porosity and permeability of the fibrous sample. This is expected because the heat of adsorption so defined in this context is a specific quantity. Although the measurement uncertainty for the average heat adsorption was estimated to be about ±15% in the precision discussion, the expected error in these correlation equations is much smaller. The average of Equations (10) and (12) (thermodynamic state heat of adsorption) are plotted in Figure 6 to compare with the reported isosteric heat of desorption (Tao et al. 1991b) that was derived from the desorption isotherms reported by Pierce and Benner (1986). This comparison shows a significant difference between the heat of adsorption and heat of desorption. In addition to the slight difference in samples (basically on the percentage of the bonding material since the bulk density does not play an important role), the main reason responsible for the difference in the heats of adsorption and desorption is the hysteresis effect. Such a large difference implies that this effect is important in the study of moisture transport in insulation. Our apparatus can be easily modified to measure the heat of desorption by passing dry air through the sample initially exposed to humid air before testing. That will be the next step in this study.

3 TRANSIENT, ONE-DIMENSIONAL HEAT AND MOISTURE TRANSPORT IN FIBERGLASS INSULATION

The problem is formulated, as a one-dimensional, transient, simultaneous heat and mass transfer problem, using the local volume averaging technique [17], as shown in Figure 7. Vapor diffusion is the mode for the moisture transport, and phase changes are caused by condensation, ablimation*

*Ablimation means a substance changing from its vapor phase to a solid phase [18].

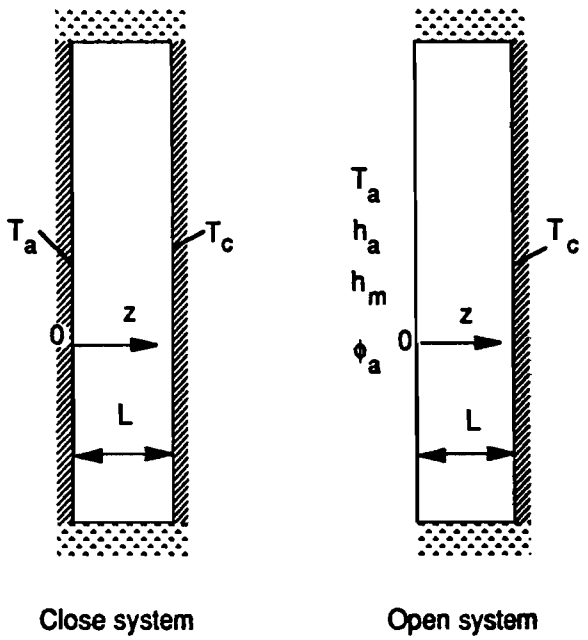

Figure 7: Transient, one-dimensional condensation, frosting and adsorption in an insulation slab for two systems: closed (a) and open (b).

and adsorption. The major assumptions made in the formulation of one-dimensional, transient heat and vapor diffusion in fibrous media are discussed in ref. [13].

3.1 Mathematical Formulation

The dimensionless forms of the governing differential equations are:
Liquid/ice phase continuity equation:

$$\frac{\partial \epsilon_\beta}{\partial t} + \frac{\dot{m}}{P_1} = 0 \tag{14}$$

Gas diffusion equation:

$$\frac{\partial(\epsilon_\gamma \rho_v)}{\partial t} - \dot{m} = \frac{\partial}{\partial z}(D_{eff}\frac{\partial \rho_v}{\partial z}) \tag{15}$$

Energy equation:

$$\rho c_p \frac{\partial T}{\partial t} + \dot{m} P_2 h' = \frac{\partial}{\partial z}(k_{eff}\frac{\partial T}{\partial z}) \tag{16}$$

where the symbols are listed in the nomenclature, the dimensionless variables and parameters are defined in Tables 1 and 2, and h' is the ratio of the heat of adsorption to the heat of condensation (or heat of sublimation). The algebraic equations of constraint are:
Volumetric constraint:

$$\epsilon_\sigma + \epsilon_\beta + \epsilon_\gamma = 1 \tag{17}$$

Thermodynamic relations:

$$p_a = p_t - p_v \tag{18}$$

$$p_a = P_3 \rho_a T \tag{19}$$

$$p_v = P_4 \rho_v T \tag{20}$$

Table 1: Dimensionless Variables

ρ	c_p	T	ρ_i	k_i	p_i	z	c_i	k_{eff}	t	$\dot{m}$
$\frac{\rho^*}{\rho_0^*}$	$\frac{c_p^*}{c_0^*}$	$\frac{T^*}{\Delta T^*}$	$\frac{\rho_i^*}{\rho_0^*}$	$\frac{k_i^*}{k_{0,eff}^*}$	$\frac{p_i^*}{p_{v,0}^*}$	$\frac{z^*}{L}$	$\frac{c_i^*}{c_0^*}$	$\frac{k_{eff}^*}{k_{0,eff}^*}$	$\frac{t^*}{L^2/\alpha_{0,eff}^*}$	$\frac{\dot{m}^*}{\rho_o^*\alpha_{0,eff}^*/L^2}$

Table 2: Dimensionless Parameters

D_{eff}	P_1		P_2		P_3	P_4	P_5	
	Liquid	Ice	Liquid	Ice			Liquid	Ice
$\frac{D_{v,eff}^*}{\alpha_{0,eff}^*}$	$\frac{\rho_\beta^*}{\rho_0^*}$	$\frac{\rho_{\beta,ice}^*}{\rho_0^*}$	$\frac{h_{fg}^*}{c_0^*\Delta T^*}$	$\frac{h_{sg}^*}{c_0^*\Delta T^*}$	$\frac{\Delta T^* R_v^* \rho_0}{p_{v,0}^*}$	$\frac{\Delta T^* R_a^* \rho_0}{p_{v,0}^*}$	$\frac{h_{fg}^*}{R_v^*\Delta T^*}$	$\frac{h_{sg}^*}{R_v^*\Delta T^*}$

and for saturation conditions

$$p_v = \exp\left[-P_5\left(\frac{1}{T} - \frac{1}{T_{ref}}\right)\right] \tag{21}$$

where

$$\rho = \epsilon_\sigma \rho_\sigma + \epsilon_\beta \rho_\beta + \epsilon_\gamma(\rho_v + \rho_a) \tag{22}$$

$$c_p = \frac{\epsilon_\sigma \rho_\sigma c_\sigma + \epsilon_\beta \rho_\beta c_\beta + \epsilon_\gamma(c_v \rho_v + c_a \rho_a)}{\rho} \tag{23}$$

$$k_{eff} = \epsilon_\sigma k_\sigma + \epsilon_\beta k_\beta + \epsilon_\gamma \frac{k_v \rho_v + k_a \rho_a}{\rho_v + \rho_a} \tag{24}$$

In the above formulation, the unknown variables are T, ρ_v, ρ_a, ϵ_β, ϵ_γ, $\dot{m}$, p_a, and p_v while all the transport and thermophysical properties for the individual phases are known from empirical data. Equations (1) – (8) can then be used to solve for these eight unknowns if the phase changes are due to condensation and frosting. However, if the adsorption process occurs, equation (8) can no longer be used to describe the local vapor density when the local relative humidity, ϕ, is less than 100 %. An alternative equation characterizing the hygroscopicity of the material is needed.

The experimental adsorption isotherms, reported by Langlais et al. [5], for fiberglass insulation seem to fit the Type II isotherms using the following BET approximation:

$$\frac{W}{W_m} = \frac{C\phi}{[1-\phi][1+(C-1)\phi]}, \tag{25}$$

where W is the mass of vapor adsorbed (adsorbate) per mass of the dry sample (adsorbent), and W_m and C are empirical constants which are generally functions of temperature and solid/gas properties. We also define:

$$W = \epsilon_\beta \rho_\beta + \epsilon_\gamma(\rho_v + \rho_a). \tag{26}$$

In this treatment, the influence of temperature on the hygroscopicity is included in the local relative humidity, ϕ. The BET equation then simply gives a relation between ϵ_β and ϕ for given W_m and C. Further information on the BET equation and the physics of W_m and C can be found in refs. [13,14]. In equation (16), the heat of adsorption is determined from the correlation, equation (10) or (12).

Two cases are considered to investigate the significance of transient hygroscopic effects with a step change in the cold boundary temperature (see Figure 7): (a) both boundaries are impermeable to water vapor flow (a closed system); (b) one boundary is impermeable and the warm boundary is open to a moist air flow (an open system). Case (a) is typical for any thermal performance test of an insulation such as for the measurement of thermal conductivity [7,8]. Case (b) is also typical to some of the practical field conditions and was studied previously [12,14]. The boundary conditions for those cases are:

Case (a):

$$T(z=0,t) = T_a, \tag{27}$$

$$\frac{\partial \rho_v(z=0,t)}{\partial z} = 0, \tag{28}$$

$$T(z=1,t) = T_c, \tag{29}$$

$$\frac{\partial \rho_v(z=1,t)}{\partial z} = 0. \tag{30}$$

If ρ_v at $z=0$ or $z=1$ reaches ρ_s, the boundary conditions (28) and (30) are replaced by $\rho_v = \rho_s$ using the saturation condition, equation (8).

Case (b):

$$\frac{\partial T(z=0,t)}{\partial z} = -Bi[T_\infty - T(z=0,t)], \tag{31}$$

$$\frac{\partial \rho_v(z=0,t)}{\partial z} = -Bi_m[\rho_\infty - \rho_v(z=0,t)], \tag{32}$$

$$T(z=L,t) = T_c, \tag{33}$$

$$\frac{\partial \rho_v(z=1,t)}{\partial z} = 0. \tag{34}$$

Again, $\rho_v = \rho_s$, using equation (8), will replace equation (25) when $\rho_v(z=1,t)$ reaches the saturated value.

The initial conditions for both cases are:

$$T(z, t=0) = T_0, \tag{35}$$

$$\rho_v(z, t=0) = \phi_0 \rho_s(T(z, t=0)), \tag{36}$$

$$\epsilon_\beta(z, t=0) = \epsilon_{\beta 0}(z). \tag{37}$$

The finite difference method is used to solve the above equations for the spatial and temporal distributions of temperature and moisture content (in terms of the volume fraction, ϵ_β). The details on computational schemes and methodology can be found in refs. [9,13].

3.2 Sample Predictions

In Figure 8, the spatial distribution of the vapor density, temperature, rate of phase change, liquid/frost volume fraction and local relative humidity for an open system, obtained numerically, are shown at various times. The profiles in the slab indicate that there can be four different phase change regions existing at the same time for $Fo > 0.117$. For example, at $Fo = 0.489$, desorption or evaporation takes place near the warm side of the slab ($z < 0.25$) where $\dot{m}$ becomes positive (Figure 8(d)), while adsorption still occurs in the middle portion of the slab, and for $z > 0.65$ condensation ($T > T_{ref}$), or ablimation ($T \leq T_{ref}$), happens. In this case, desorption or evaporation, near the warm side, is observed because ϕ_a is near 1.0. For cases with $\phi_a < 0.8$, this region is still in adsorption (see the broken line in Figure 8(d)). The desorption and evaporation cause a decrease in ϵ_β as Fo increases (see Figure 8(c) for $z < 0.25$ and $Fo = 0.489$), and the maximum accumulation of water is near the cold side of the slab.

4 COMPARISON OF PREDICTION WITH EXPERIMENTAL DATA

Experiments were performed to measure the temperature and moisture distribution in a typical medium-density fiberglass insulation slab, using an apparatus as shown in Figure 9 [11]. The glass-fiber slab is initially dried in an oven at 105 ^{o}C for about 15 hours, and then wrapped by a plastic sheet and cooled to the room temperature. After the slab is properly mounted in the apparatus, moist air in the duct and the coolant in the heat exchanger are supplied at the same time. The air temperature and humidity and the cold temperature are stabilized within 10 to 15 minutes. The temperatures of the glass-fiber slab, air and cold plate are recorded and monitored by a personal computer through a data acquisition unit. A typical experiment runs about 3 to 4 hours which covers both a transient and a quasi-steady-state period. At a desired time, the slab is taken out the apparatus and each layer is weighed using an electronic scale, to find a total amount of moisture/frost accumulation during that period of time. For the purpose of comparison, we also perform the same experiments for dry specimens in which the slab is completely wrapped with plastic sheets and the test is run at a low ambient humidity and the same air flow rate and air temperature.

From the experiments, the time variation of the temperature field in the slab, the time variation of the heat flux at the cold side of the slab, and the moisture/frost accumulation can be obtained for various air velocities, temperatures, relative humidities, and cold-plate temperatures. In order to investigate the effects of moisture accumulation on the heat loss through insulation, a heat flux ratio Q' is defined as

$$Q' = \frac{\left(k_{eff}\frac{\partial T}{\partial z}\right)_{z=1}}{\left(k_{\rm dry}\frac{\partial T}{\partial z}\right)_{z=1,\rm dry}}, \tag{38}$$

which is defined as the ratio of the heat flux, Q, to the heat flux for the same slab at a completely dry condition (i.e., $\phi_a = \phi_0 = 0$) and otherwise the same initial and boundary conditions.

4.1 Temperature and Heat Flux

The typical time variation of the heat flux at the cold boundary and the temperature field are shown in Figs. 10 and 11 for the cases of a closed system and an open system, where the dimensionless heat flux Q is defined as

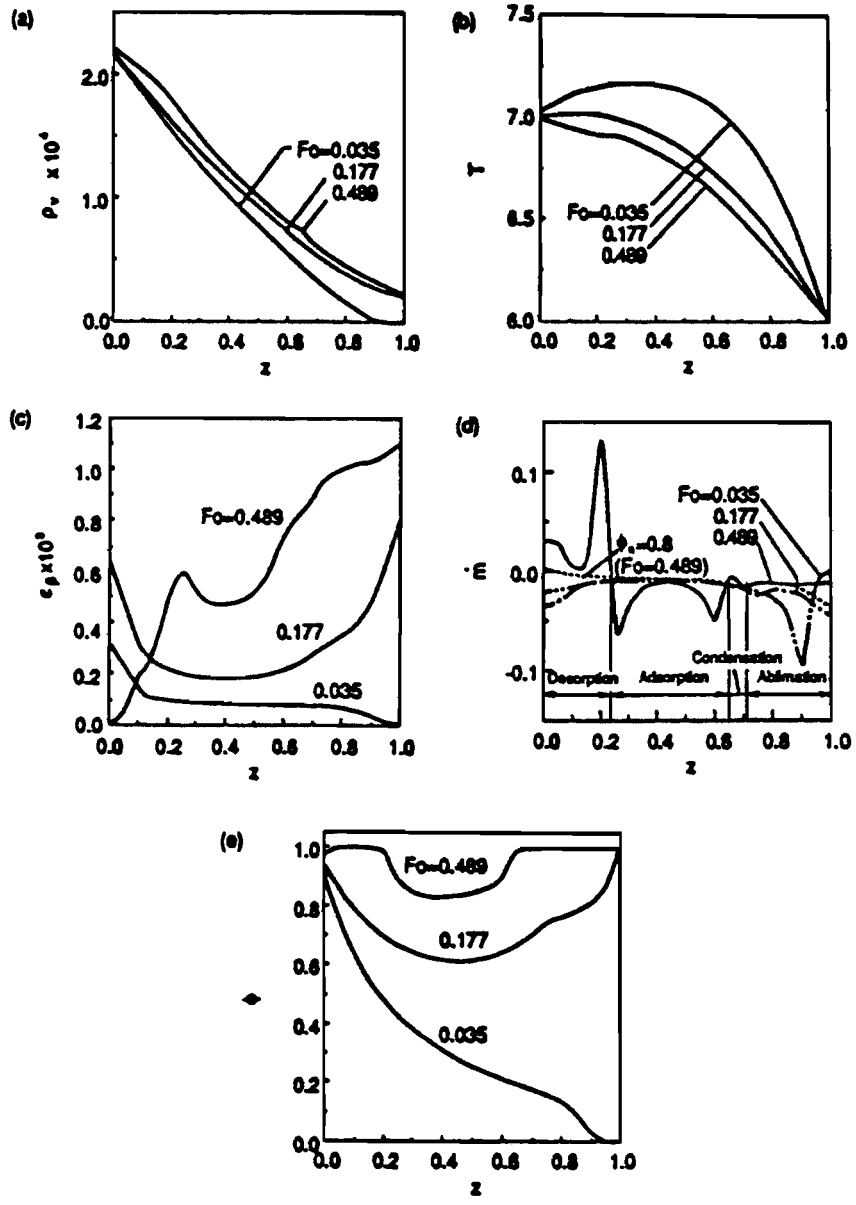

Figure 8: Spatial distributions of (a) ρ_v, (b) T, (c) ϵ_β, (d) $\dot{m}$ and (e) ϕ: $\phi_a = 0.97$, $T_c^* = 252$ K for the BET II approximation. The broken line is for $\dot{m}$ at $\phi_a = 0.80$ when $Fo = 0.489$.

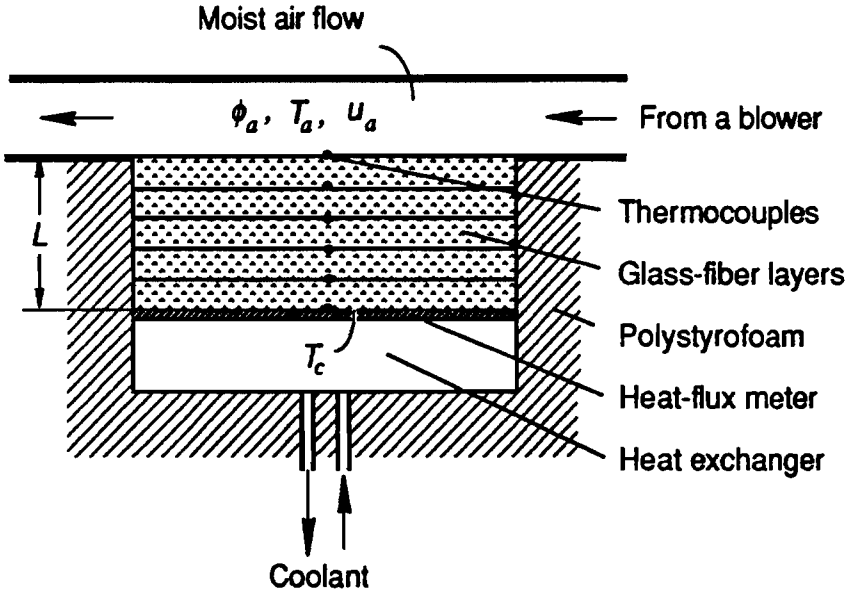

Figure 9: A schematic of the experimental apparatus.

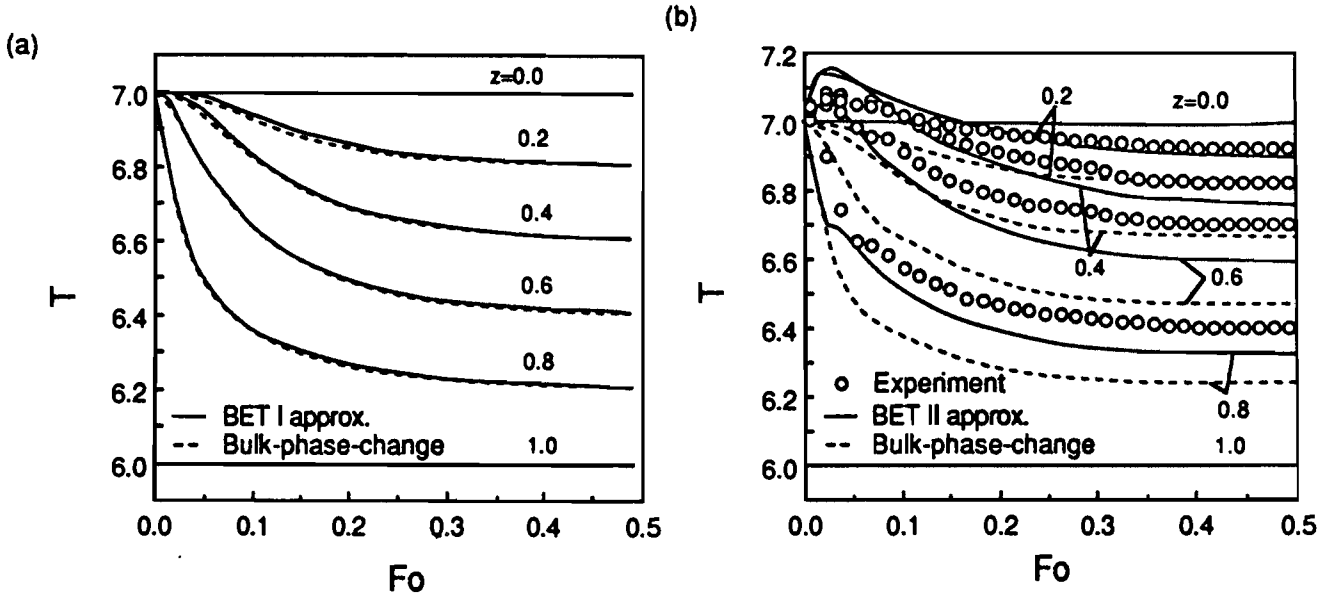

Figure 10: Time variation of the temperature for (a) a closed system : $\phi_0 = 0.1$ and $T_c^* = 252$ K, and (b) for an open system: $\phi_a = 0.80$, $T_c^* = 252$K.

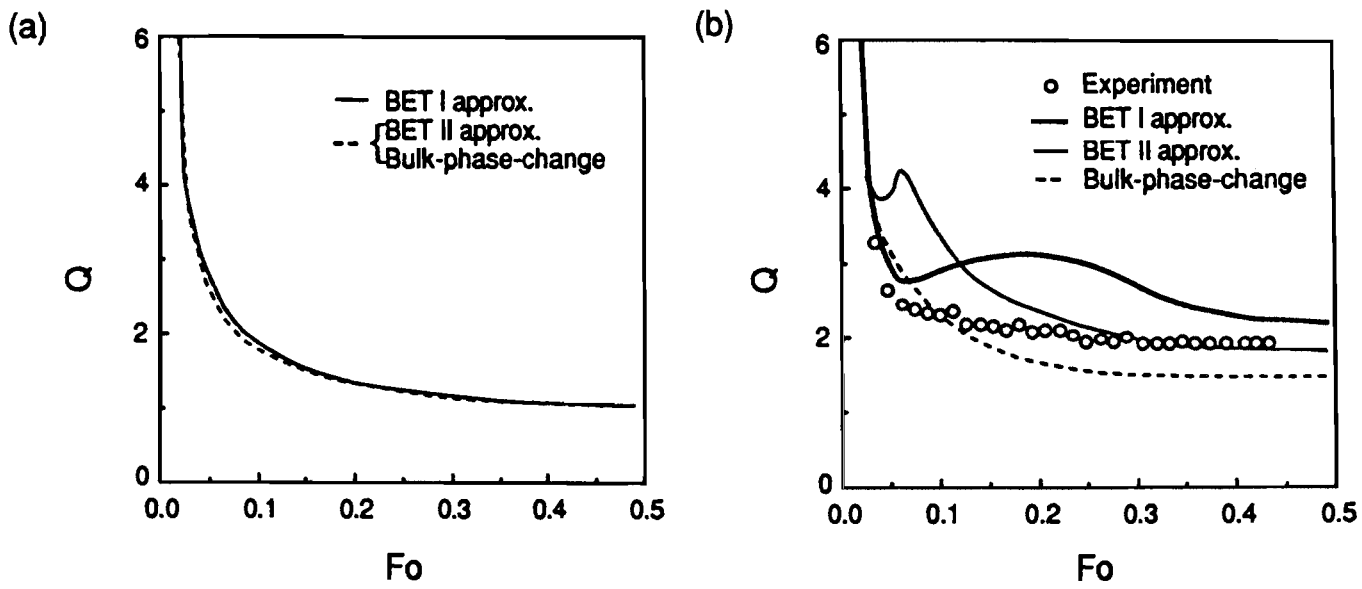

Figure 11: Time variation of the temperature for (a) a closed system : $\phi_0 = 0.1$ and $T_c^* = 252$ K, and (b) for an open system: $\phi_a = 0.80$, $T_c^* = 252$K.

$$Q = -k_{eff} \left. \frac{\partial T}{\partial z} \right|_{z=1} \tag{39}$$

The results obtained from the adsorption model and the bulk-phase-change model are essentially the same for a closed system. Since there is no external vapor supply, the amount of moisture that can migrate within the slab depends entirely on the initial water vapor content. In the example shown in Figure 10(a), $\phi_0 = 0.1$ is used which corresponds to an initial ϵ_β of approximately 2.6×10^{-4}, which is not small compared to the criterion set in [9,10]. The temperature field is not significantly influenced by the hygroscopicity of the fibers; i.e., results for the BET I are very similar to the case of no hygroscopic effects (the difference between the results from the BET II approximation and the bulk-phase-model are unnoticeable in Figure 10(a)). This supports the experimental results for a closed system [13] in which no significant effects of hygroscopicity were shown for a medium-dry-density glass-fiber insulation.

On the other hand, when the external vapor is allowed to diffuse into the slab as in an open system, the effects of hygroscopicity on the temperature field become important. As shown in Figure 9(b), the heat flux, using the adsorption model, is higher than the prediction based on the bulk-phase-change model with no hygroscopic effects. For the adsorption model, the results for the BET I approximation (high hygroscopicity) is larger than that for the BET II approximation (low hygroscopicity). This is, of course, because of the heat source effects of phase change which increase the local temperature as seen in Figure 10(b). The enhancement of adsorption, due to the external vapor diffusion, increases the amount of this internal heating as compared with the closed system. The alteration of the temperature field causes a time delay in reaching a quasi-steady state. From Figure 10(b), it can be seen that, according to the bulk-phase-change model, the Fourier number, at a quasi-steady-state, is about 0.2, while the adsorption model predicts it to be greater than 0.33. The experimental results of the heat flux and the temperature distribution are also shown in Figs. 10 and 11. It is obvious that the experimental data agree better with the adsorption model, in spite of the uncertainties in the adsorption properties that were extrapolated for the

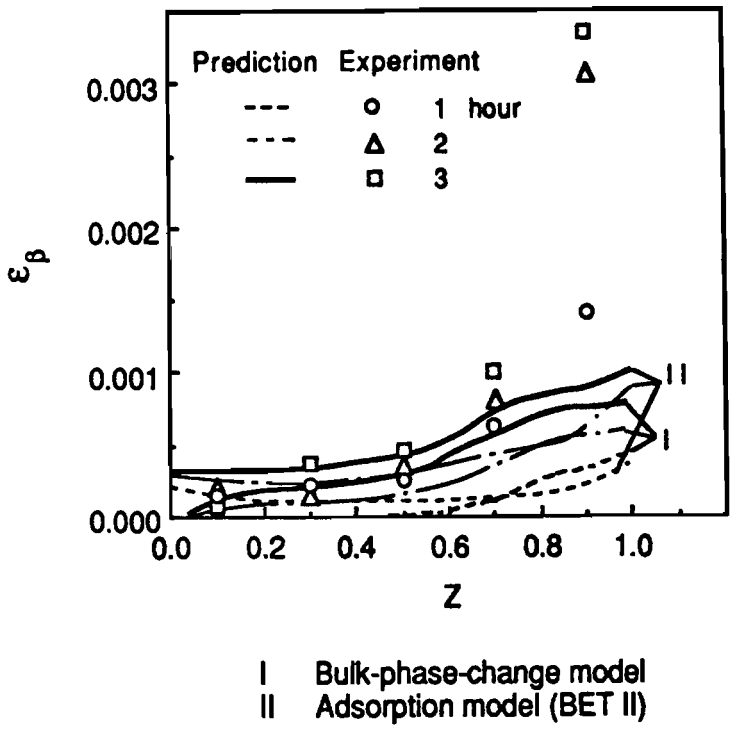

Figure 12: Spatial distributions of ϵ_β obtained from the bulk-phase-change model, adsorption model and experiments.

test conditions. It is interesting to note that the quasi-steady-state values for Q and T, calculated from these two models, are different. This is because the predicted moisture accumulation from the two models is different, as it can be seen from Figure 11. The measured moisture accumulation is closer to the prediction by the adsorption model. The discrepancy in ϵ_β near the cold boundary (z=0.9), at a sub-freezing temperature, is due to the formation of a frost layer on the cold plate of the heat-flux meter. The effect of this boundary condition on the analytical formulation is discussed later. Putting this aside, we can then conclude that when heat and mass transfer are coupled in a transport process in porous media, which have hygroscopic effects, one can not neglect the hygroscopic effects in predicting the temperature and heat flux. As indicated by the typical example shown in Figure 10(b), the discrepancy in Q can be up to 50 % at $Fo = 0.23$. Even at the quasi-steady state, it is still around 30 %.

It is shown that, compared to a dry slab, the heat loss from the cold side can be double due to phase changes in an open system. Also Q' is larger at a higher ϕ_a for the sub-freezing temperature. For the cold temperature above 273.16 K and for $Fo > 0.35$, the heat-flux ratio, Q', as a function of Fo, shows some abrupt changes which results in Q', at $\phi_a = 0.8$, being less than Q', at $\phi_a = 0.5$. This behavior is mainly due to the temperature variation near the cold boundary, which is influenced by the transition from physical adsorption to bulk condensation and ablimation. This transition occurs when the local relative humidity becomes greater than 0.95. As discussed in [13], the time required for a local relative humidity to reach 0.95 depends on the temperature difference across the slab and the capacity of the insulation slab for hygroscopicity with a complex interaction among heat and mass transfer and phase change. Qualitatively, the trends, shown in Figure 12, indicate that hygroscopicity has a stronger effect on the heat flux for the case with the cold temperature above the triple point of water than that with a sub-freezing temperature. As a comparison, the quasi-steady-state heat flux ratio for non-hygroscopic insulation, obtained from the

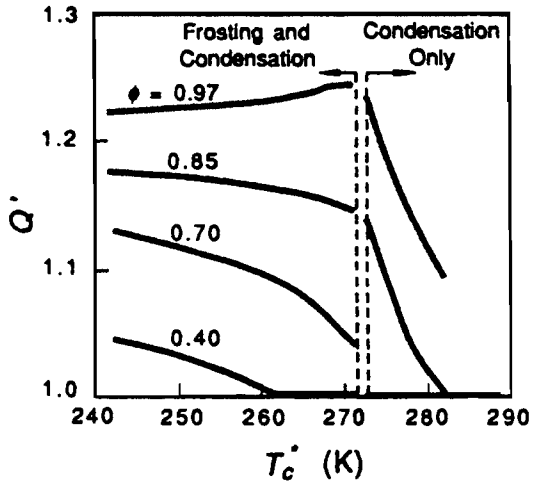

Figure 13: The effect of cold temperature T_c^* on the quasi-steady-state heat flux ratio for different ambient relative humidities (for non-hygroscopic fibers): $\epsilon_{\beta 0} = 10^{-7}$

bulk-phase model, is shown in Figure 13 as a function of the cold temperature and ambient relative humidity. This information will provide a guide for analyzing the transport process involved in fiberglass insulation.

4.2 Impermeable Boundary Conditions

In the above numerical modelling, the boundary at the cold side of insulation is modelled as impermeable. This specification creates some real problems when the experimental data were collected. It was observed that, due to the uneven nature of fiberglass slab surfaces, an air gap of the order of 1 mm on average, inevitably exists between the slab and the cold, impermeable plate. When the cold surface temperature falls below freezing, a frost layer can form on the cold plate. This is also a common phenomenon in practical conditions. It was found that the above numerical results under-predicted the frost accumulation near the cold surface of the insulation slab and the boundary conditions need to be modified [19]. In Figure 14, the results with the modified boundary conditions are presented and compared with the measured data. A good agreement has been achieved.

5 SUMMARY

A study of heat and moisture transport in a glass-fiber insulation slab is performed to measure the heat of adsorption and to investigate the effects of hygroscopicity, condensation and frosting on the thermal performance of fiberglass insulation. For the transport processes involved, phase changes and latent heat transfer are caused by bulk condensation and frosting as well as physical adsorption

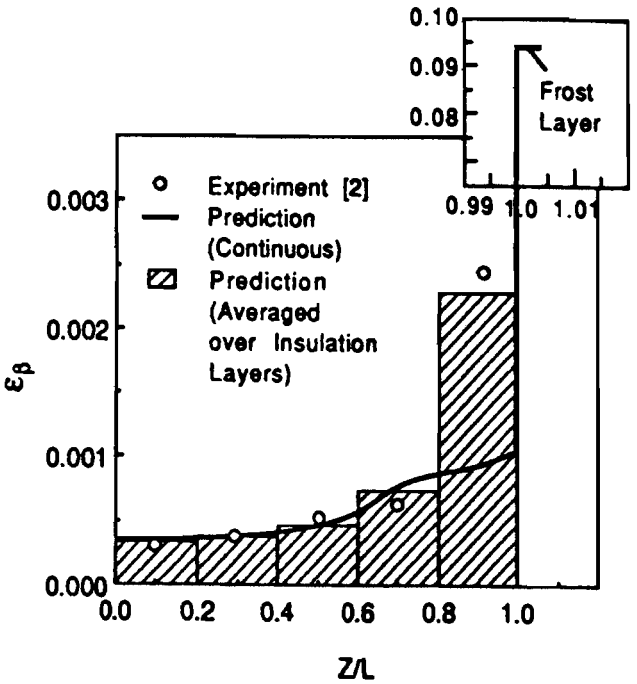

Figure 14: Comparison of the predicted ϵ_β, using the modified boundary condition, with the measured data.

and capillary condensation (hygroscopicity effects). Given the comparisons between the adsorption model, the bulk-phase-change model and experimental results, the following conclusions may be drawn for typical glass-fiber insulation:

(a) For an initially dry glass-fiber insulation with medium density, the effects of hygroscopicity on the temperature field and heat loss are negligible, if the sample is isolated from the ambient mass transfer; however, these effects are very significant when one side of the same fibrous slab is open to moist air during a transport process.

(b) For an open system, the discrepancy between the adsorption model and the bulk-phase-change model can be as high as 30 % for the quasi-steady-state heat flux. The measured heat flux and temperature distribution support the adsorption model based on the BET II approximation for low adsorption effects.

(c) The frost accumulation results in an increase in the heat flux ratio, Q', as compared to the process when only condensation takes place, if the ambient relative humidity is approximately above 0.40 (Figure 13).

6 NOMENCLATURE

Bi	Biot number, $h_a L/k^*_{eff}$
Bi_m	mass transfer Biot number, $h_m L/D^*_{v,eff}$
C	empirical constant in equation (12)
c_p	heat capacity at constant pressure
D_{eff}	dimensionless diffusivity, $D^*_{v,eff}/\alpha^*_{0,eff}$

$D^*_{v,eff}$	effective vapor diffusivity, m^2s^{-1}
Fo	Fourier number, $\alpha^*_{0,eff}t^*/L^2$
h^*_a	heat transfer coefficient, W m^{-2} K^{-1}
h^*_{fg}	enthalpy of vaporization, J kg^{-1}
h^*_m	mass transfer coefficient, m s^{-1}
h^*_{sg}	enthalpy of sublimation, J kg^{-1}
k	thermal conductivity
L	characteristic length of the slab, m
$\dot{m}$	rate of phase change
p	pressure
$\dot{q}''$	heat flux, W m^{-2}
Q	dimensionless heat flux
Q'	heat-flux ratio defined in equation (30)
R^*_a	air gas constant, J kg^{-1} K^{-1}
R^*_v	water vapor gas constant, J kg^{-1} K^{-1}
t	time
T	temperature
ΔT^*	reference temperature difference, $T^*_a - T^*_c$, K
W	water content per unit dry mass
W_m	empirical constant in equation (12)
z	coordinate axis

Greek Symbols

$\alpha^*_{0,eff}$	effective thermal diffusivity, m^2s^{-1}
ϵ	volume fraction
ϕ	relative humidity
ρ	density
τ	tortuosity

Subscripts

a	air
c	cold
ref	reference
s	saturated
t	total
v	vapor phase
β	liquid or ice phase
γ	gas phase which consists of air and water vapor
σ	solid phase
0	initial; reference for non-dimensional scales (Table 2)

Superscripts

$'$	ratio
$*$	dimensional

7 REFERENCES

1. *Water in Exterior Walls: Problems and Solutions*, ASTM STP 1107 (1991).

2. C. Langlais, M. Hyrien, and S. Karlsfeld, Moisture migration in fibrous insulating material under the influence of a thermal gradient, *Moisture Migration in Buildings*, ASTM STP **779**, 191-206 (1982).

3. D. A. Pierce, and S. M. Benner, Thermally induced hygroscopic mass transfer in a fibrous medium, *Int. J. Heat Mass Transfer*, **29**, 1683-1694 (1986).

4. M. K. Kumaran, Moisture transport through glass-fibre insulation in the presence of a thermal gradient, *Journal of Thermal Insulation*, **10**, 243-255 (1987).

5. N. E. Wijeysundera, M. N. A. Hawlader and Y. T. Tan, Water vapor diffusion and condensation in fibrous insulations, *Int. J. Heat Mass Transfer*, **32**, 1865-1878 (1989).

6. K. Vafai and S. Sarker, Condensation effects in a fibrous insulation slab, *J. Heat Transfer*, **108**, 667-675 (1986).

7. K. Vafai and H. C. Tien, A numerical investigation of phase change effects in porous materials, *Int. J. Heat Mass Transfer*, **32**, 1261-1277 (1989).

8. H. C. Tien and K. Vafai, A synthesis of infiltration effects on an insulation matrix, *Int. J. Heat Mass Transfer*, **33**, 1263-1280 (1990).

9. Y.-X. Tao, R. W. Besant, and K. S. Rezkallah, Unsteady heat and mass transfer with phase change in an insulation slab: frosting effects, *Int. J. Heat Mass Transfer*, **34**, in press (1991).

10. G. P. Mitalas, and M. K. Kumaran, Simultaneous heat and moisture transport through glass-fibre insulation: an investigation of the effect of hygroscopicity, *The 1987 ASME WAM-SED*, Vol. 4, pp. 1-4, ASME (1987).

11. Y.-X. Tao, R. W. Besant, and K. S. Rezkallah, Heat and moisture transport through a glass-fiber slab with one side subject to a freezing temperature, *Water in Exterior Walls: Problems and Solutions*, ASTM STP 1107, in press (1991).

12. F. A. L. Dullien, *Porous media: Fluid Transport and Pore Structure*, pp. 70-71. Academic Press, New York (1979).

13. Y.-X. Tao, R. W. Besant, and K. S. Rezkallah, The transient thermal response of a glass-fiber insulation slab with hygroscopicity effects, *Int. J. Heat Mass Transfer*, in press (1992).

14. S. G. Gregg, and K. S. W. Sing, *Adsorption, Surface Area and Porosity*, p. 17. Academic Press, London (1982).

15. S. Ross, and J. P. Olivier, *On physical adsorption*, p. 81. New York: John Wiley & Sons (1964).

16. Y.-X. Tao, R. W. Besant, and C. J. Simmonson, Measurement of the heat of adsorption for a typical fibrous insulation, *ASHRAE Trans.*, **98**, Pt. 2 (1992).

17. S. Whitaker, Simultaneous heat, mass and momentum transfer in porous media: a theory of drying, In *Advanced in Heat Transfer* (Edited by J. P. Hartnett and T. F. Irvine, Jr.), Vol. 13, Academic Press, New York (1977).

18. A. V. Luikov, *Heat and Mass Transfer in Capillary-porous Bodies*, (Translated by P. W. B. Harrison and Translation Edited by W. M. Pun), p. 254. Pergamon Press, Oxford (1966).

19. Y.-X. Tao, R. W. Besant, and K. S. Rezkallah, Modelling of frost accumulation in a fibrous insulation slab and on an adjacent cold plate, *Int. Comm. Heat Mass Transfer*, **18** 609-618 (1991).